Letter

Separating spin dynamics modes in iron oxide nanoparticles

M. Zobel,[1,2,*] M. Appel,[3] S. L. J. Thomä,[4] M. Plekhanov,[2] and A. Magerl[1,5]
[1]*JCNS-3: Neutron Analytics for Energy Research, Forschungszentrum Jülich GmbH, Wilhelm-Johnen-Straße, D-52428 Jülich, Germany*
[2]*Institute of Crystallography, RWTH Aachen University, Jägerstrasse 17–19, D-52066 Aachen, Germany*
[3]*Institute Max von Laue–Paul Langevin, 71 avenue Martyrs, F-38000 Grenoble, France*
[4]*Swiss Federal Laboratories for Materials Science and Technology, EMPA, Überlandstrasse 129, CH-8600 Dübendorf, Switzerland*
[5]*Friedrich-Alexander-Universität Erlangen-Nürnberg, Physics Department, Biophysics Group, Henkestraße 91, D-91052 Erlangen, Germany*

(Received 26 July 2024; accepted 3 February 2025; published 11 February 2025)

The different modes of the spin dynamics in ferrimagnetic magnetite iron oxide nanoparticles (Fe_3O_4) have been addressed by μeV neutron spectroscopy for particles with a diameter of 75 ± 18 Å. In an approach building on intensity considerations over a wide range of wave vectors Q in combination with diffusion dynamics, we identify three magnetic modes prevailing in distinct Q regimes up to 1.7 Å^{-1}: (i) Evaluating the structure factor of quasielastic magnetic intensity enables to identify uniquely longitudinal superparamagnetic spin fluctuations in the small Q regime < 0.5 Å^{-1}, (ii) individual spin relaxation with quasielastic intensity albeit of low intensity is present in two Q ranges of 0.5 Å^{-1} $< Q < 1.0$ Å^{-1} and 1.5 Å^{-1} $< Q < 1.7$ Å^{-1}, and (iii) a surprisingly low-energy inelastic spin excitation of 23.2 μeV in magnetite IONPs is found at 150 K in the magnetic Bragg region between 1.1 Å^{-1} $< Q < 1.4$ Å^{-1}. Its temperature dependence suggests a collapse of the coherent transverse magnetic fluctuations and a transition into a generalized diffusive mode at about 500 K.

DOI: 10.1103/PhysRevB.111.L060406

Introduction. Iron oxide nanoparticles (IONPs) show magnetic properties markedly different from the bulk [1]. A unique feature is the superparamagnetic state playing a fundamental role when IONPs are used, e.g., as a contrast agent for magnetic resonance tomography (MRT), for medical imaging or in hyperthermia [2]. At sufficiently high temperatures when the thermal energy exceeds the magnetic anisotropy energy, the orientation of the single domain magnetic spin will fluctuate in an isotropic diffusive manner between the easy directions. The large amplitude motion, also termed longitudinal spin dynamics, will no longer be observable when the relaxation time becomes longer than the time resolution of the experimental method used. The corresponding temperature is usually termed blocking temperature. In real systems the blocking temperature may be smeared out because of particle inhomogeneities such as size distribution and in consequence a smearing of the anisotropy energy, phase purity, or canted spins in a surface shell of the nanoparticle. When the thermal energy is low, there are still precession modes of the magnetization vector around the easy axes of the magnetic structure [3]. These transverse collective magnetic modes or spin wave excitations are most readily apparent at a magnetic Bragg peak and thus carry a wave vector $Q_{sw} = 0$. They have been experimentally observed by neutron spectroscopy at the position of the first magnetic Bragg peak with an energy level of 250 μeV at low temperature in antiferromagnetic hematite (α-Fe_2O_3) nanoparticles with 150 Å diameter [4] and with a splitting of about 50 μeV (upon extrapolation from measurements in an external magnetic field) in maghemite (γ-Fe_2O_3) nanoparticles with 84.2 Å edge length [5]. Here, we report on the spin dynamics over a continuous Q range up to up to 1.7 Å^{-1}, in which different modes of spin dynamics become visible.

Experiment. Citrate-capped IONPs with a diameter of 75 ± 18 Å according to dynamic light scattering equilibrated for 48 h at 8% relative H_2O humidity synthesized according to the procedure described in Ref. [6] were studied. They are in the shape of truncated octahedra with hexagonal facets and the ligand coverage is 2.8 ligand/nm^2 [7]. IONPs mainly crystallize as magnetite ($Fd\bar{3}m$ space group). However, during storage in air, 10–30 wt % of the maghemite ($P4_32_11$) phase may appear. More details can be found in Ref. [5]. For sample shipment and during the measurements the sample had been placed in a sealed Al container to protect it from environmental humidity.

The instrument BATS (the backscattering and time-of-flight spectrometer) at the Institute Max von Laue-Paul Langevin in Grenoble, France, is a newly installed high-resolution neutron spectrometer in inverted geometry with a fast chopper system in the primary instrument and standard

*Contact author: m.zobel@fz-juelich.de, she/her

Published by the American Physical Society under the terms of the Creative Commons Attribution 4.0 International license. Further distribution of this work must maintain attribution to the author(s) and the published article's title, journal citation, and DOI.

TABLE I. List of Q values on BATS in Å^{-1}.

$Q1$	$Q2$	$Q3$	$Q4$	$Q5$	$Q6$	$Q7$	$Q8$	$Q9$	$Q10$	$Q11$	$Q12$	$Q13$	$Q14$	$Q15$
0.19	0.29	0.44	0.64	0.85	0.94	1.03	1.13	1.22	1.31	1.39	1.47	1.54	1.62	1.68

Si 111 crystal analyzers in the secondary instrument. The setting used provided a full width at half maximum (FWHM) resolution of 3.2 μeV corresponding to timescale of 2.6 ns, and an energy transfer range from −143 to +186 μeV [8].

The angular scattering range on BATS is presented by 15 Q values (wave vector transfer) given in Table I.

Results and discussion. Figure 1 shows selected spectra taken at $Q = 0.19$, 0.94, 1.31, and 1.62 Å^{-1}. The data are fitted with a Delta function (black) and one Lorentzian (green), both convoluted with the experimentally measured resolution function obtained from a sample data set at 2 K. In addition, a constant background (dashed black) has been added. For the fitting, the whole measured energy range from −143 to + 186 μeV has been used, while the plots are limited to ±70 μeV for increased clarity of the graphs. The ordinates are scaled to identical values with respect to a vanadium data set used for intensity normalization. The full y coordinate in Fig. 1 corresponds to about 1% of the peak intensity at zero energy transfer for the smallest Q value = 0.19 Å^{-1}.

The spectra show dynamic intensities in addition to the elastic component at all Q values (Figs. 1 and 2). This extra intensity is significant in the small Q regime [Fig. 1(a)], becomes very weak in the medium Q range [Fig. 1(b)], and is prominent again in the region of the magnetic 111 Bragg peak [Fig. 1(c)]. Beyond this, it drops again to a low level [Fig. 1(d)].

The full Q dependences of the elastic intensity and of the excess intensity are shown in Figs. 2(a) and 2(b), respectively. Based on the behavior of the excess intensity we identify four Q regimes as shown in Fig. 2(b) [(1) region A: 0.19–0.29 Å^{-1}, corresponding to $Q1$–$Q2$; (2) region B: 0.62–1.03 Å^{-1}, corresponding to $Q4$–$Q7$; (3) region C: 1.22–1.38 Å^{-1}, corresponding to $Q9$–$Q11$; and (4) region D: 1.55–1.68 Å^{-1}, corresponding to $Q13$–$Q15$] while disregarding in the following the transition regions.

Region A. The excess intensities in region A are well described by a Lorentzian function also nominated quasielastic scattering representative for a diffusion process [Fig. 1(a)].

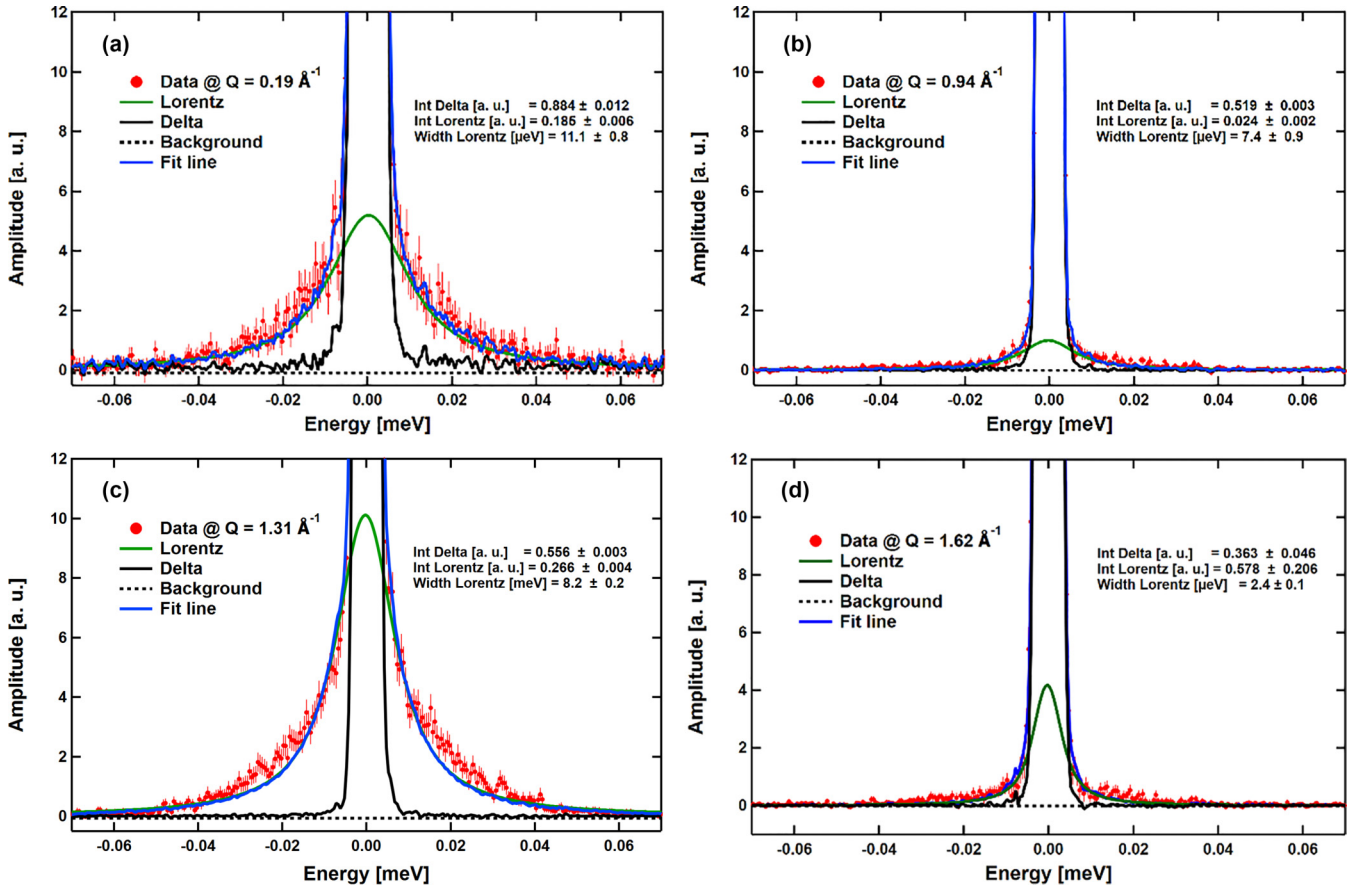


FIG. 1. Selected spectra at $Q = 0.19$, 0.94, 1.31, and 1.62 Å^{-1} at 150 K fitted with a Delta (black line) and a Lorentz function (green line), both convoluted with the experimental resolution plus a constant background (dashed black). The ordinates are scaled to satisfy vanadium normalization.

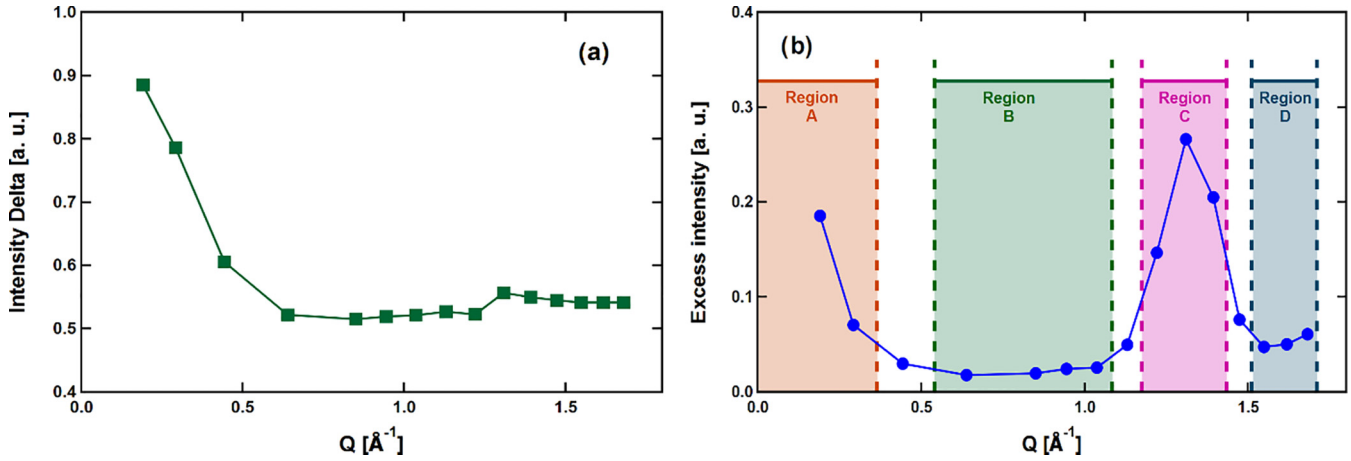


FIG. 2. Q dependence of the intensities of the elastic component of the spectra (Delta function) (a) and of the dynamic scattering in excess of the elastic scattering (b).

The average half width at half maximum (HWHW) of 10.7 ± 0.5 μeV corresponds to a relaxation time of 0.063 ns. The relaxation times of citrate and water motions on the surface of IONPs at 360 K of 2.3 ± 1.1 and 0.05 ± 0.02 ns, respectively, are considerably longer [9]. In consequence, the observed relaxation time at 150 K is too fast as to be associated with an atomic or molecular hydrogen-related motion of the IONP. However, they may well be of magnetic origin.

The intensity of this quasielastic magnetic component decays rapidly with increasing Q [Fig. 2(b)], evidently in a similar fashion as the decay of the truly elastic intensity which originates from nuclear small angle scattering from the IONPs [Fig. 2(a)]. Although the Q range accessible on BATS does not extend to small enough Q values for a precise determination of a particle size, we deduce from the noted similarity that the origin of the dynamic component stems from large entities of correlated spins similar in size to the nanoparticles themselves [10]. Based primarily on this structure factor argument in combination with the fast dynamic aspect we assign the origin of the quasielastic scattering in region A to superparamagnetic relaxations.

It was shown, e.g., by Mössbauer spectroscopy and in superconducting quantum interference device (SQUID) measurements, that 5–10 nm magnetite IONPs exhibit superparamagnetic behavior [2,11]. However, the structure factor argument evoked here allows to establish a direct relation with the shape of the superparamagnetic entity.

Regions B and D. The spectra region B [Fig. 1(b)] and region D [Fig. 1(d)] have a similar appearance and shall be discussed together. The salient feature in these regimes is the low excess intensities with little variation with Q. A description of the spectra with one Lorentzian function representative for a diffusive process appears appropriate, albeit a precise shape determination is difficult in view of the low count numbers. The Lorentzian linewidths in region B are between 3.9 and 11.5 μeV (including error bars) with an average value of 7.7 μeV and this connects with the linewidths in region D, which are between 2.8 and 5.6 μeV with an average value 3.8 μeV. In view of the overlapping values of the Lorentzian widths combined with the low quasielastic intensities with weak Q dependence over both ranges, the origin of the excess intensities can be assigned to the same dynamical process. It is suggestive to ascribe it to isolated spin dynamics in the magnetic shell englobing the coherent superparamagnetic kernel of the nanoparticles [12,13], maybe in a state resembling a spin glass arrangement.

Region C. A description of the spectra with one Lorentzian function fails in region C [Fig. 1(c)]. Trying to amend the dissatisfactory model by adding a second Lorentzian centered at the elastic position still does not represent an adequate fitting. Alternatively, a description involving one Lorentzian at the elastic position representing diffusion plus a damped oscillator function [14] signifying a spin excitation is appropriate as shown in Fig. 3(a) for $Q10$. Thus, the scattering law $S(Q, \hbar\omega)$ for the total excess intensity in region C is given by

$$S(Q,\hbar\omega) = \frac{\mathrm{LF}}{\pi}\frac{\Gamma}{(\hbar\omega)^2+\Gamma^2} + \frac{\mathrm{DOF}}{\pi}\frac{2\gamma(\hbar\omega_M)^2}{[(\hbar\omega)^2-(\hbar\omega_M)^2]^2+4\gamma^2(\hbar\omega)^2}, \quad (1)$$

with LF and DOF representing the amplitudes of the Lorentzian and oscillator functions, Γ and γ are the corresponding HWHM and damping parameter, and $\hbar\omega_M$ is the oscillator energy. For the fitting, these functions have been convoluted with the experimentally measured resolution. Further a (small) constant background has been allowed.

The same approach is to be applied for the two neighboring Q values $Q9$ and $Q11$, i.e., in the entire regime of the magnetic Bragg peak, proving the presence of two magnetic phenomena in the region C. For more distant Q values from the Bragg peak there is no indication for inelastic scattering. All three Q values in the Bragg region give within errors consistently an excitation energy of 23.2 ± 0.4 μeV with a damping constant of 16.3 ± 0.9 μeV at 150 K. Calculating an effective internal magnetic anisotropy field B_{eff} from the oscillator energy according to

$$\hbar\omega = g\mu_B B_{\mathrm{eff}}\,, \quad (2)$$

with the Landé factor $g = 2$ and the Bohr magneton $\mu_B = 5.79 \times 10^{-5}\,\mathrm{eV\,T^{-1}}$ yields $B_{\mathrm{eff}} = 0.20\,\mathrm{T}$.

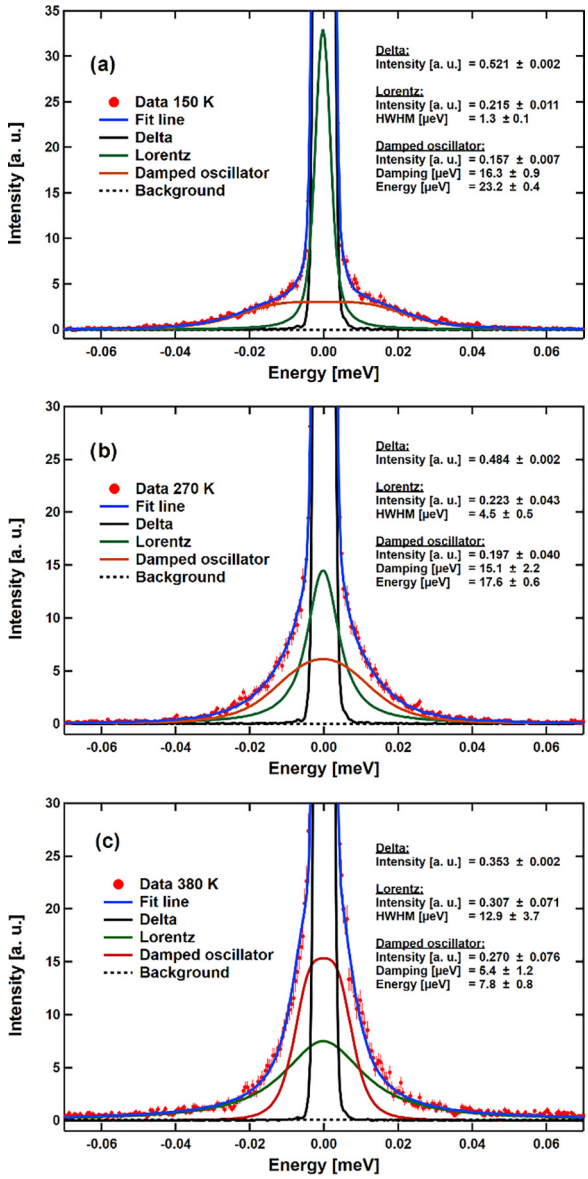


FIG. 3. Temperature dependence of selected spectra for the region C of magnetic Bragg scattering ($Q10$) fitted with an elastic component (black line), one Lorentzian line (green), and a damped oscillator function (brown), all convoluted with the experimentally measured resolution. In addition, a constant background was allowed (black dashed). The y range shown corresponds to about 7% of the full scale.

While spin excitations at 300 K have been reported at a higher energy of 250 μeV for hematite and of 50 μeV for maghemite nanoparticles (from an extrapolation of measurements with an applied external field) [4,5,15], this is an observation for an excited spin state in magnetite IONPs, which is also notable because of its very low-energy level.

A selective description of the temperature dependence of the spectra at $Q10$ is shown in Fig. 3 with the individual contributions of the coherent spin excitation and the diffusive component. This procedure is needed for temperatures up to 330 K, whereas data at 360 and 380 K are equally well described by one Lorentzian function only due to a reduced value of oscillator energy with rising temperature. The temperature behavior of the kinetic parameters of the oscillator function is shown in Fig. 4.

The excitation energy of the coherent transversal spin state becomes reduced with rising temperature [Fig. 4(a)], indicating the influence of thermal fluctuations. At the highest temperature of 380 K, the gap energy is reduced to the 7.8 ± 0.8 μeV corresponding to an anisotropy field of 0.07 T. A linear extrapolation of the excitation energy according to Ref. [3] reaches a zero value at about 500 K [Fig. 4(a)], indicating a breakdown of the transversal spin wave state at this point and a transition to a common relaxation description where the distinction between longitudinal and transversal dynamics merge into a single isotropic regime [16].

The damping of $\gamma = 16.3 \pm 0.9$ μeV at 150 K [Fig. 4(b)] suggests a (transversal) lifetime $\tau = \frac{\hbar}{\gamma} = 40$ ps. The damping becomes reduced with increasing temperature and reaches a value of 5.4 ± 1.2 μeV at 380 K. At the same time the Lorentzian HWHM Γ increases with temperature in a way that damping γ and HWHM Γ have comparable values at the higher temperatures. Hence, the two processes merge into a single relaxation mode as already suggested by the vanishing gap energy [Fig. 4(a)].

We note that hydrogen-related diffusion may become of relevance at 380 K, which cannot be separated dynamically within the present scheme [9]. However, the relatively strong magnetic intensity at the magnetic Bragg peak makes it unlikely that these are of relevance for the present discussion of region C.

Summary. High-resolution neutron spectroscopy on IONPs at 150 K shows extra intensity in the entire Q range in addition to elastic scattering. A feature exploited here is a pronounced variation of this feature as a function of Q, which allows to identify three different modes of spin excitations:

(i) A strong quasielastic component representing a diffusive mode is observed at small Q values. The pronounced rise at small Q shows that a structure similar in size to the nanoparticles themselves is at the origin of the magnetic phenomenon, and we recognize this as an experimental observation of the most evident signature of superparamagnetic fluctuations.

(ii) The quasielastic scattering in regions B and D at 150 K with a linewidth narrower than the superparamagnetic dynamics is small in intensity and lacks a pronounced Q variation. For this reason, it is associated with isolated spin dynamics in the magnetic shell of the nanoparticles.

(iii) The region of the magnetic Bragg peak features two components, one being quasielastic from longitudinal fluctuations of the paramagnetic spin. The second component is inelastic representing a low-energy transversal spin excitation with an effective magnetic anisotropy field of 0.20 T at 150 K. The temperature dependence of both spin modes suggests a transition into an isotropic diffusion state above room temperature.

Acknowledgments. We gratefully acknowledge inspiring discussions with Th. Brückel and K. Lefmann. We further acknowledge funding by the Deutsche Forschungsgemeinschaft (DFG, German Research Foundation) via ZO 369/3–1 and we are grateful for beamtime INTER-528 at IN16B at ILL [17].

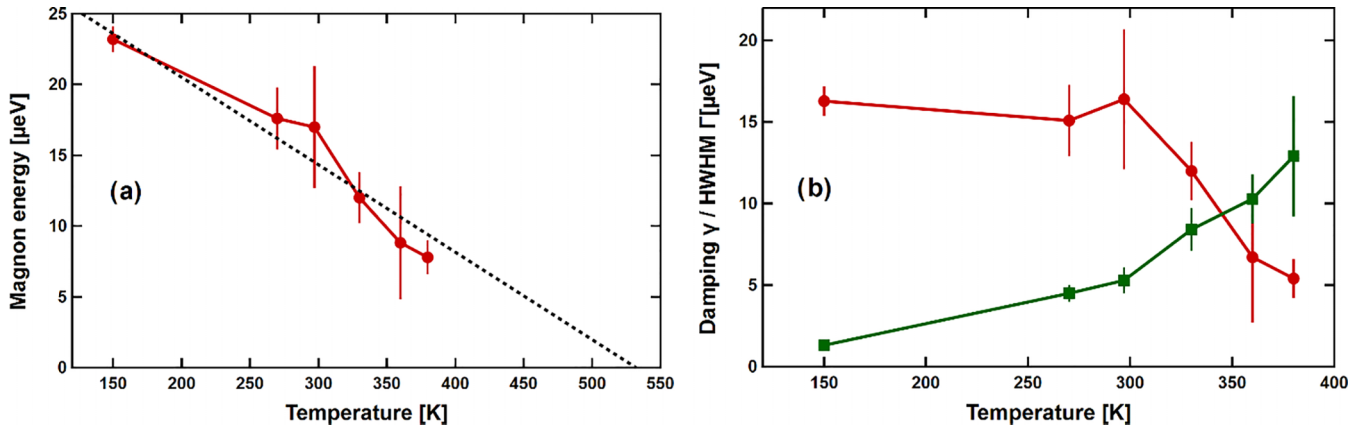


FIG. 4. Temperature dependence of the kinetic properties of the spin excitations at the Bragg peak: (a) Magnon energy according to the damped oscillator function and its linear extrapolation to zero value at $T \sim 500$ K (dashed line). (b) Damping parameter γ of the damped oscillator function (red dots) and HWHM Γ of the Lorentzian contribution (green squares).

[1] S. Bader, *Colloquium*: Opportunities in nanomagnetism, Rev. Mod. Phys. **78**, 1 (2006).

[2] I. Hilger and W. A. Kaiser, Iron oxide-based nanostructures for MRI and magnetic hyperthermia, Nanomedicine **7**, 1443 (2012).

[3] S. Mørup and B. R. Hansen, Uniform magnetic excitations in nanoparticles, Phys. Rev. B **72**, 024418 (2005).

[4] M. F. Hansen, F. Bødker, S. Mørup, K. Lefmann, K. N. Clausen, and P. A. Lindgård, Dynamics of magnetic nanoparticles studied by neutron scattering, Phys. Rev. Lett. **79**, 4910 (1997).

[5] S. Disch, R. P. Hermann, E. Wetterskog, A. A. Podlesnyak, K. An, T. Hyeon, G. Salazar-Alvarez, L. Bergstrom, and Th. Bruckel, Spin excitations in cubic maghemite nanoparticles studied by time-of-flight neutron spectroscopy, Phys. Rev. B **89**, 064402 (2014).

[6] M. Eckardt, S. L. J. Thomä, M. Dulle, G. Hörner, B. Weber, S. Förster, and M. Zobel, Long-term colloidally stable aqueous dispersions of $\leqslant$5 nm spinel ferrite nanoparticles, ChemistryOpen **9**, 1214 (2020).

[7] S. L. J. Thomä, S. W. Krauss, M. Eckardt, P. Chater, and M. Zobel, Atomic insight into hydration shells around facetted nanoparticles, Nat. Commun. **10**, 995 (2019).

[8] M. Appel, B. Frick, and A. Magerl, First Results with the Neutron Backscattering and TOF Spectrometer Option BATS on IN16B, Physica B Condens. Matter **562**, 6 (2019).

[9] M. S. Plekhanov, S. L. J. Thomä, A. Magerl, M. Appel, and M. Zobel, Quasi-elastic neutron scattering of citrate-capped iron oxide nanoparticles: Distinguishing between ligand, water, and magnetic dynamics, J. Phys. Chem. C **128**, 11661 (2024).

[10] M. Hennion, C. Bellouard, I. Mirebeau, J. L. Dormann, and M. Nogues, Dual spin dynamics of small Fe particles, Europhys. Lett. **25**, 43 (1994).

[11] M. Mikhaylova, D. K. Kim, N. Bobrysheva, M. Osmolowsky, V. Semenov, T. Tsakalakos, and M. Muhammed, Superparamagnetism of magnetite nanoparticles: Dependence on surface modification, Langmuir **20**, 2472 (2004).

[12] S. Disch, E. Wetterskog, R. P. Hermann, A. Wiedenmann, U. Vainio, G. Salazar-Alvarez, L. Bergström, and Th. Brückel, Quantitative spatial magnetization distribution in iron oxide nanocubes and nanospheres by polarized small-angle neutron scattering, New J. Phys. **14**, 13025 (2012).

[13] D. Zákutná, N. Rouzbeh, D. Nižňanský, J. Duchoň, A. Qdemat, E. Kentzinger, and D. Honecker, Magnetic coupling in cobalt-doped iron oxide core–shell nanoparticles: Exchange pinning through epitaxial alignment, Chem. Mater. **35**, 2302 (2023).

[14] For example, see P.-A. Lindgård, in *Spin Waves and Magnetic Excitations 1*, edited by A. S. Borovik-Romanov and S. K. Sinha (Elsevier, New York, 1988), p. 287.

[15] K. Lefmann, F. Bødker, S. N. Klausen, M. F. Hansen, K. N. Clausen, P.-A. Lindgård, and S. Mørup, A neutron scattering study of spin precession in ferrimagnetic maghemite nanoparticles, Europhys. Lett. **54**, 526 (2001).

[16] W. F. Brown, Jr., Thermal fluctuations of a single-domain particle, Phys. Rev. **130**, 1677 (1963).

[17] https://doi.ill.fr/10.5291/ILL-DATA.INTER-528.